Numerical Analysis of Tiros Radiation Observations

By
Ferdinand Baer
and
William Kamm

Technical Paper No. 67
Department of Atmospheric Science
Colorado State University
Fort Collins, Colorado

Colorado State University

Department of Atmospheric Science

Paper No. 67

NUMERICAL ANALYSIS OF TIROS RADIATION OBSERVATIONS

by

Ferdinand Baer
and
William Kamm

Technical Paper No. 67
Department of Atmospheric Science
Colorado State University
Fort Collins, Colorado

June 1965

NUMERICAL ANALYSIS OF TIROS RADIATION OBSERVATIONS*

by

Ferdinand Baer
and
William Kamm

Abstract

TIROS III radiation measurements are taken from binary tape, selected for a given geographic region, accepted under satisfactory model conditions and interpolated to points for which no fix is given. These raw data are then fit to a uniformly spaced set of grid points covering the region of interest. The fitting procedure is either a least squares polynomial fit or a weight function fit, the choice depending on the nature of the data in the influence region about the grid point. A sample analysis and statistical information on data distribution are presented to suggest the effectiveness of the analysis procedure to the type of data under consideration.

*A report on research conducted in support of the CSU project on the Meteorology of the Southeast Asia Summer Monsoon [DA 28-043-AMC-01303 (E)].

1. INTRODUCTION

Information received from meteorological satellites may have substantial utility to both the forecaster and the research worker. Direct photographic data give an immediate visual display of cloud patterns with their associated hydrometeorological events. A more systematic coverage of the earth's radiation properties is given by the continuous scanning of satellite-mounted radiometers. Analysis of this recorded data, with its broad spatial and temporal coverage, can lead to improved understanding of some of the more intractable atmospheric problems. Tracking major storm centers, distinguishing rainfall regions and observing diurnal variations in cloud patterns are just a few of the purposes to which satellite data may be applied.

Perhaps the utility of satellite data is not limited by any paucity of significant problems but rather by the obstacles encountered in data reduction. Radiation data are digitalized and made available in binary form on magnetic tape. With a thorough understanding of the format in which the data is presented, it may be extracted -- with suitable computing equipment -- and consequently employed for meteorological purposes. It is the purpose of the subsequent discussion to show, by application to a particular example, that satellite-radiation data may be made available for convenient analysis of specific problems directly from a computer without burdensome human intervention. Such data preparation allows the meteorological analyst to concentrate on the primary physical problem to which he plans to apply his data.

Analysis of a number of TIROS III orbits will be considered in the sequel. This analysis involves the extraction of data (confined to radiation information from Channel II), evaluation of its significance, establishment of the geographic location to which it is applicable, and an interpolation procedure which will assign a radiation value to a selected set of geographic points. The final outcome of this procedure will be a map with radiation values established on a grid of equally spaced points; these maps may be hand analysed or analysed by machine. Since the satellite orbit is of reasonably short duration (≈ 90 minutes) and since the geographic region of interest is confined (to Southeast Asia), these maps may be considered Eulerian maps.

II. INFORMATION EVALUATION

TIROS III was a space oriented, axially rotating satellite with floor and wall radiometer sensors. In its orbital progression, many possible combinations of earth viewing were achieved; some, more valuable than others. Because of the satellite's rotation, the sensors -- set at 45 degrees to the satellite axis -- scanned a significant path during each cycle. The possible scanning modes of the sensors and their progression are shown in Figure 1 and are defined in terms of a nadir angle. This nadir angle (α) describes the angular distance between the point on earth being scanned and the satellite azimuthal point; clearly when both sensors are recording, each has an associated nadir angle. We note the three possible modal conditions: single open, closed, and alternating open. In the closed mode either the floor or the wall sensor scans the earth during the entire cycle; in the open mode either of the sensors scans the earth during part of the cycle while scanning space during the remaining part of the cycle, thus intercepting the horizon; in the alternating mode both floor and wall sensors scan either different or the same regions of the earth.

The initial selection of data was based on the requirement that only when the satellite was scanning in the single open mode was data accepted. The selection rule was applied to the nadir angle by the formula,

$$\alpha < 90^\circ - \tan^{-1} (R/\sqrt{2\,RH + H^2}) \approx 26^\circ$$

where the value of 26 degrees was determined for the satellite height, H = 717 km, and the mean radius (R) of the earth; one can see from Figure 1 that this value of α will confine data to the single open mode.

Observation of several analyses implied that insufficient data, because of the above constraint, was available over the geographical region of interest. Furthermore, it was pointed out that data in the alternating open mode was satisfactory except in the region ($\alpha > 40^\circ$) where both sensors viewed the same region on earth. This latter restriction is due to the disparity in recording between the floor and wall sensors.

Changing the condition on α to $\alpha \leq 40^\circ$ allows inclusion of the adequate part of the alternating mode but restricts the data beyond the undesirable overlap region. Fortunately, since data from both sensors is utilized and since the swaths are short in the far edge of the alternating mode, not much data is lost. However, the new condition allows data from the closed mode also. Since in the closed mode no horizon is available for reference, there appears to be some question as to the accuracy of locating measurements. The errors which may then arise have not yet been well defined and may not be of great significance. In consequence of our need for more data and the questionable error possibilities, we have accepted the closed mode data on the assumption that subsequently applied smoothing procedures would possibly counteract any errors in data location.

The orbits which are used in this analysis are listed in Table 1. The sensors, which are recording black-body radiation temperature in the 8 - 12 μ region (Channel II) show a degradation with increasing orbit number (Bandeen, et al., 1963). Figure 2 shows the required correction as a function of temperature for a number of orbits. Noting the linearity of the curves in this figure, a linear regression curve was computed for each orbit. Thus for orbit i,

$$T_i \text{ (corrected)} = A_i + B_i \, T_i \text{ (recorded)} \qquad (1)$$

The coefficients of equation (1) are listed in Table 1. Radiation values finally used are computed from the black-body temperature (corrected) by the well-known formula,

$$R = T^4 \text{ (corrected)} \times 8.132 \times 10^{-11}$$

As the satellite progresses in its orbit, it scans the earth during each cycle in a "swath"; in closed mode the swath includes coverage of the earth during the entire cycle whereas in open mode part of the scan is toward space. Every fifth sensor record during a swath is assigned a geographic location; i. e., the location of the sensed point on earth is defined. However, intermediate points which are scanned are not located and their positions must be interpolated. The change in position from one geographically

TABLE 1

Orbit numbers, linear regression coefficients, minimum longitude, maximum longitude, number of data points, number of computed grid points.

Orbit #	A_i	B_i	λ max	λ min	Data Points	Computed grid points
1. 63	-05.2225	1.03619	138.0	67.5	4887	3864
2. 77	-05.9475	1.04179	138.0	70.5	5000	3810
3. 91	-06.6450	1.04738	154.0	72.0	4901	3739
4. 105	-07.1950	1.05250	156.0	75.0	4681	3568
5. 119	-07.8725	1.05804	157.0	79.5	4655	3261
6. 133	-08.3850	1.06274	147.0	84.0	4534	3174
7. 134	-08.4525	1.06321	121.0	58.0	4504	3111
8. 148	-08.8450	1.06738	101.0	62.5	4284	2935
9. 176	-09.8975	1.07679	128.0	70.0	3808	2604
10. *183	-09.4200	1.07548	116.0	76.5	2140	1938
11. 190	-10.3075	1.08083	130.5	73.5	3601	2405
12. 218	-11.1800	1.08887	139.5	83.5	2724	2566
13. 261	-12.4975	1.10119	124.5	75.0	2140	2170
14. 282	-13.1275	1.10696	114.0	65.5	2137	2349
15. 381	-15.1850	1.12774	117.0	65.0	2918	2435
16. 409	-15.6750	1.13250	125.0	68.0	2551	2417
17. *445	-16.2075	1.13768	100.5	61.5	1601	2048
18. 480	-16.6025	1.14196	111.5	58.5	5000	3026
19. *501	-16.8583	1.14458	134.0	79.5	2241	2602
20. *544	-17.1150	1.14851	124.0	60.0	1877	2224
21. 579	-17.2700	1.15143	114.0	64.5	2654	1688
22. *600	-17.4025	1.15321	137.0	82.5	3328	2750
23. 607	-17.5425	1.15417	120.5	68.5	2452	1688
24. *614	-17.4125	1.15405	138.5	85.0	3931	2437
25. *628	-17.5175	1.15542	140.0	82.5	3453	2190
26. *642	-17.5575	1.15643	142.5	87.5	3563	2171
27. *671	-17.6275	1.15821	123.5	74.0	3114	1999
28. *685	-17.6100	1.15899	125.5	77.5	2815	1896
29. *713	-17.8850	1.16149	133.5	92.5	2287	1700
30. *727	-18.1550	1.16327	136.5	100.0	1891	1496
31. *742	-18.1975	1.16429	114.5	83.0	1487	1120
32. *756	-18.3725	1.16554	117.5	90.0	1165	898
33. *770	-18.4600	1.16649	121.5	97.5	907	732
34. 798	-18.9675	1.16982	129.5	85.0	1324	1182
35. *812	-18.8550	1.17012	133.5	122.0	896	144

*These orbits were run using single open mode only.

defined viewing to the next is caused by two motions, the satellite's orbital motion and its rotation rate. Both of these motions are considered constant over the interval considered. Let us define the following notation:

λ_i ≡ Longitude of scanned point

θ_i ≡ Latitude of scanned point

λ_{si} ≡ Longitude of corresponding subsatellite point

θ_{si} ≡ Latitude of corresponding subsatellite point

λ_{i+5} ≡ Longitude of subsequently defined scanned point

etc.

The location of these points may be seen on Figure 3. To isolate the separate motions referred to above, the satellite orbital motion is subtracted from the coordinate at the $(i+5)^{th}$ position. Thus the $(i+5)^{th}$ position without satellite translation is given as,

$$\hat{\theta}_{i+5} = \theta_{i+5} - (\theta_{s(i+5)} - \theta_{si})$$
$$\hat{\lambda}_{i+5} = \lambda_{i+5} - (\lambda_{s(i+5)} - \lambda_{si}) \qquad (2)$$

Since the translation has been removed, we may deal with the satellite spin about the axis through $(\lambda_{si}, \theta_{si})$. The radial distance from this subsatellite point to the two successively recorded points (λ_i, θ_i), $(\hat{\lambda}_{i+5}, \hat{\theta}_{i+5})$ may be calculated from known values by the formulae (where the distance has been normalized by the earth's mean radius),

$$r_i = [(\theta_{si} - \theta_i)^2 + (\lambda_i - \lambda_{si})^2 \cos^2 \theta_i]^{\frac{1}{2}}$$
$$r_{i+5} = [(\theta_{si} - \hat{\theta}_{i+5})^2 + (\hat{\lambda}_{i+5} - \lambda_{si})^2 \cos^2 \hat{\theta}_{i+5}]^{\frac{1}{2}} \qquad (3)$$

On the assumption that the radial distance changes linearly as the satellite views from point i to $i+5$,

$$r_{i+j} = r_i - j/5\,(r_i - r_{i+5}), \quad 0 \leq j \leq 5. \tag{4}$$

The angular distances between the meridians through the points (θ_i, λ_i), $(\hat{\theta}_{i+5}, \hat{\lambda}_{i+5})$ and the radial lines through $(\lambda_{si}, \theta_{si})$ denoted by β_i, β_{i+5} (see Figure 3) are calculated by the formulae,

$$\begin{aligned} \beta_i &= \tan^{-1}\,[(\lambda_i - \lambda_{si})\cos\theta_i/(\theta_{si} - \theta_i)] \\ \beta_{i+5} &= \tan^{-1}\,[(\lambda_{i+5} - \lambda_{si})\cos\hat{\theta}_{i+5}/(\theta_{si} - \hat{\theta}_{i+5})] \end{aligned} \tag{5}$$

Again assuming linear changes in β from i to $i+5$, the intermediate angles become,

$$\beta_{i+j} = \beta_i + j/5\,(\beta_{i+5} - \beta_i) \quad 0 \leq j \leq 5 \tag{6}$$

Equations (4) and (6) now allow us to calculate the latitude and longitude of the intermediate (j) points. We must, however, add the satellite's translation. This procedure yields the coordinates of the intermediate points (and thus of all points for which radiometer sensing is available) from the relations,

$$\begin{aligned} \theta_{i+j} &= \theta_{si} - r_{i+j}\cos\beta_{i+j} + j/5\,(\theta_{s(i+5)} - \theta_{si}) \\ \lambda_{i+j} &= \lambda_{si} + \frac{r_{i+j}\sin\beta_{i+j}}{\cos\theta_{i+j}} + \frac{i}{5}\,(\lambda_{s(i+5)} - \lambda_{si}) \end{aligned} \tag{7}$$

To each sensed point for which coordinates are assigned, there is associated a subsidiary (and different) nadir angle defined as $\hat{\alpha}$. This nadir angle is the angular distance between the point being sensed and the azimuthal point of the satellite. Should this angle become large, the error in the geographic location of the sensed point becomes

intolerably large. Thus no data is accepted unless this angle (for which linear interpolation is also applied at those points with no specified coordinates), is less than 55 degrees ($\hat{\alpha} < 55°$).

III. NUMERICAL ANALYSIS

With the considerations of the last section, it is now possible to extract radiation data with its corresponding coordinates. We select data which falls into the geographic region

$$\lambda_{min} \leq \lambda \leq \lambda_{max} \; ; \; \theta_{min} \leq \theta \leq \theta_{max}$$

The extreme values used in the investigation are listed in Appendix A. The radiation values over this region are not necessarily uniformly distributed; consequently we establish a uniform grid of points over the region. These grid points are spaced at intervals $\Delta\lambda = \Delta\theta$ (defined in Appendix A).

Since the data density about most grid points is reasonably high (as will be seen subsequently), we have elected to fit the data about each grid point to a quadratic surface with the grid point at the origin. This procedure has been frequently used in meteorological analyses; see for example Gilchrist and Cressman (1954) and Johnson (1957). Let us denote the distances from any data point (subscripted with i) to a grid point (subscripted with g)as,

$$x_i = (\lambda_i - \lambda_g) \cos \frac{(\theta_i + \theta_g)}{2}$$

$$y_i = \theta_i - \theta_g \qquad (8)$$

We now assume that the radiation values in the vicinity of the grid point can be expressed by the analytical function

$$R(x, y) = \sum_{l} \sum_{m} a_{l,m} x^{l} y^{m} \quad l + m \leq 2 \tag{9}$$

where the $a_{l,m}$ are as yet arbitrary but will be chosen by the method of least squares to best fit the data. Since we are interested only in $R(0, 0)$ -- at the location of the grid point -- we need evaluate only $a_{0,0}$. By the method of least squares,

$$\delta \sum_{i} [R_i - R(x_i, y_i)]^2 = 0 \tag{10}$$

where the R_i in equation (10) refer to the data points to which equation (9) will be fit, $R(x_i, y_i)$ is given by equation (9), and the summation over i covers all data points in the allowed region of influence. The variation is clearly applied to the coefficients $a_{l,m}$. Applying the variation in equation (10) and noting that each of the variations $\delta a_{l,m}$ is independent, we arrive at the set of equations which range over all combinations of l, m (clearly six in the case of a quadratic surface),

$$\sum_{l'} \sum_{m'} a_{l',m'} \left[\sum_{i} x_i^{l+l'} y_i^{m+m'} \right] = \sum_{i} R_i x_i^{l} y_i^{m} \tag{11}$$

Equation (11) may be recognized as a matrix equation with columns given by combinations of (l, m) and rows given by combinations of (l', m'). The bracketed factor on the left hand side is a square matrix (6 x 6) and by inversion of this matrix we may solve for the coefficients $a_{l',m'}$. The solution of this equation for $a_{0,0}$ was carried out by using the method of Crout (1941). The coordinate values for determining the solution of equation (11) are established from equation (8).

To establish the relevant data points, an influence region about each grid point must be selected. The size of this region will be determined by the amount of smoothing desired or by the

data density. The influence region used in the present discussion was chosen as an almost square region about the grid points subject to the conditions

$$\left.\begin{aligned} |\lambda_i - \lambda_d| \\ |y_i - y_d| \end{aligned}\right\} \leq d \qquad (12)$$

where the influence parameter $d = 2.5\ \Delta\lambda$ (also listed in Appendix A). The influence region and the character of the grid may be seen on Figure 4.

It is well known that six data points are necessary to fit a quadratic surface. Should all these points lie on a conic section, however, the surface is indeterminate. The probability that all the data points will lie on a conic section obviously decreases with increasing number of data points. To minimize this possibility and yet to avoid oversmoothing in regions of low data density, we require that at least eight pieces of data lie in the influence region for any one grid point. If this condition is not met, no value is computed for the grid point.

Although an adequate number of data points in the influence region is a necessary condition for computing a grid value, it is by no means sufficient. Should the data all be clustered in one quadrant or should they be distributed on the periphery of the influence region, our expectation of a meaningful computation for the grid value would be small indeed. The following further constraints are applied to the data.

a) Unless at least one data point lies in each of the four quadrants surrounding the grid point, no calculation is performed. This requirement assures that the surface to be fit at least covers the grid points.

b) The center of gravity of the data points must lie within the square region about the grid point as described in Figure 4. The center of gravity condition may be expressed analytically by the inequality,

$$\frac{\sum_{L=1}^{N} x_i}{N}, \frac{\sum_{L=1}^{N} y_i}{N} \leq \Delta\theta = \Delta y \tag{13}$$

Thus the center of gravity for any one grid point cannot fall beyond any neighboring grid point. If it does, no calculation is performed.

Data satisfying the above constraints should yield reasonable grid point values. However, should the interpolated grid point value exceed the mean value of the data in the influence region by an excessive amount, we assume the polynomial fitting technique is unsatisfactory and use a weight function method instead. The factor which the evaluated grid point must satisfy is derived from a distribution of some sample data. We require that the difference between the computed value and the mean value of the data points not exceed twice the standard deviation of the sample data. Thus on the assumption that the sample data represents reasonably well all our data, we question calculated values only if they fall into the range of the extreme five per cent of our data sample. The value (γ) is listed in Appendix A.

The influence region and the conditions on data points are the same for the weight function method as for the polynomial fitting method. However, the radiation value at the grid point, R(0, 0), is computed from the data values by the formulae,

$$R_g(0,0) = \frac{\sum_i W_i R_i}{\sum_i W_i} \tag{14}$$

and the weight function is defined so that it has a magnitude of two at the origin and zero at the extremes of the influence region. This function, expressed analytically as,

$$W_i = 2 - \frac{|x_i| + |y_i|}{d} \tag{15}$$

may be seen graphically in Figure 5. The isolines of the weight function appear as the perimeter of squres rotated by 45 degrees about the origin.

Should the value thus computed by the weighting method also exceed the mean value of the data points by the same constant which disallowed the polynomial fitting method, the computed grid point value is discarded and no assignment is made for the grid point.

IV. ANALYSIS CHARACTERISTICS

The entire data population over the assigned region, for any orbit, cannot exceed 5000 because of computational limitations. This amount is rarely reached, as can be seen from the population counts in Table 1; moreover, by noting the longitudinal range for each orbit listed in Table 1 and the latitudinal range (Appendix A), the density afforded by 5000 data points is, to say the least, adequate. We note from the information of Section III that the effects of a data point may be felt at several grid points. Should we wish merely to have interpolation density without smoothing, the number of computed grid points should equal the number of data points. If the number of grid points exceeds the number of data points, some overspecification is implied but may be accepted because of smoothing. The number of grid points for which successful calculations are performed is listed in Table 1 for all orbits.

As an example of the type maps which are created by the analysis program herein described, Figure 6 shows an analyzed radiation map for orbit 77. The map shows that the analysis procedure yields patterns which are not meteorologically outrageous; gradients are realistic and comparison with cloud maps shows a good correlation. In terms of the grid established for this orbit, note the extensive regions over which no analysis could be performed. To understand the data density associated with the orbital maps better, Figure 7 describes, in analysed form, this data density in terms of the number of data points in the influence region of each grid point. We note high density of data along the edges of the analyzed regions. This density is strongly suggestive that the satellite is in closed mode over a large region. The assumption of closed mode is also consistent with the angular view of a satellite swath in this mode as calculated from the satellite height and nadir angle. Without this closed mode data, little analysis could be performed. Yet, upon inspection of Figure 6, we do do not see any obvious disparity between the analysis in the closed mode and that in the open mode (northeast and southwest portions of the map). Over a sizeable area strong data smoothing was applied,

as noted from large values for data density. Such smoothing may be advantageous insofar as instrumental errors would thus be minimized. However, under strong smoothing conditions, tight gradients are difficult to observe.

The frequency of radiation values for a selected number of orbits (taken from the computed grid point values) may be seen from Figure 8. The purpose of this figure in our discussion is to describe the variation and magnitude of the physical variable under analysis. Any evaluation of the parameter itself will involve physical considerations which are not under consideration herein. The frequency of data points in the influence region for the orbits described in Figure 8 are displayed in Figure 9. There appears to be no significant correlation between data distribution and frequency of data points per grid point, an observation which might have been anticipated. It is interesting to note, however, that most of the grid points evaluated were amply supplied with data.

V. ACKNOWLEDGEMENTS

A considerable amount of machine programing for this analysis was performed by Mrs. Pat White. Some fifteen hours of IBM-7094 machine time was provided through the facilities of the Western Data Processing Center, Graduate School of Business Administration, University of California, Los Angeles. Raw data was provided by the Physics Branch of the National Aeronautics and Space Administration, Goddard Space Flight Center.

REFERENCES

Bandeen, W. R., et al, 1963: TIROS IV Radiation Data Catalog and Users' Manual. NASA, Goddard Space Flight Center, Greenbelt, Maryland, 250 pp.

Crout, P. D., 1941: A short method for evaluating determinants and solving systems of linear equations with real or complex coefficients. Trans. AIEE, 60. 1235-1241.

Gilchrist, B., G. P. Cressman, 1954: An experiment in objective analysis. Tellus, 6, 309-318.

Johnson, D. H., 1957: Preliminary research in objective analysis. Tellus, 9, 316-322.

APPENDIX A

Limits applied in the analysis:

θ_{max} = 32° N. Lat.

θ_{min} = 8° S. Lat.

λ_{min} = 200° long.

$\Delta\lambda = \Delta\theta$ = 0.5° grid interval

d = 1.25° influence factor

γ = .1345 in radiation units

APPENDIX B

FLOW DIAGRAM

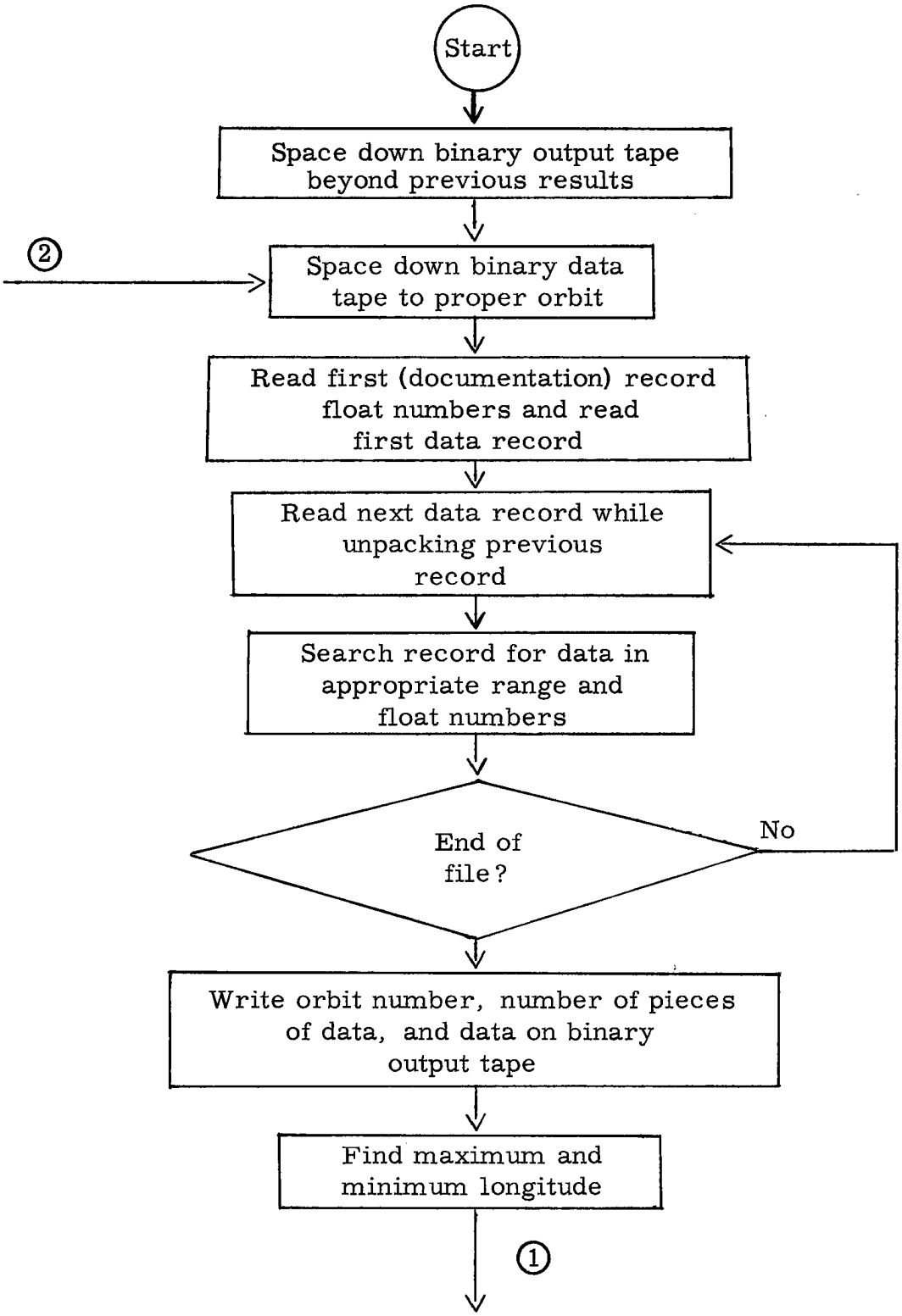

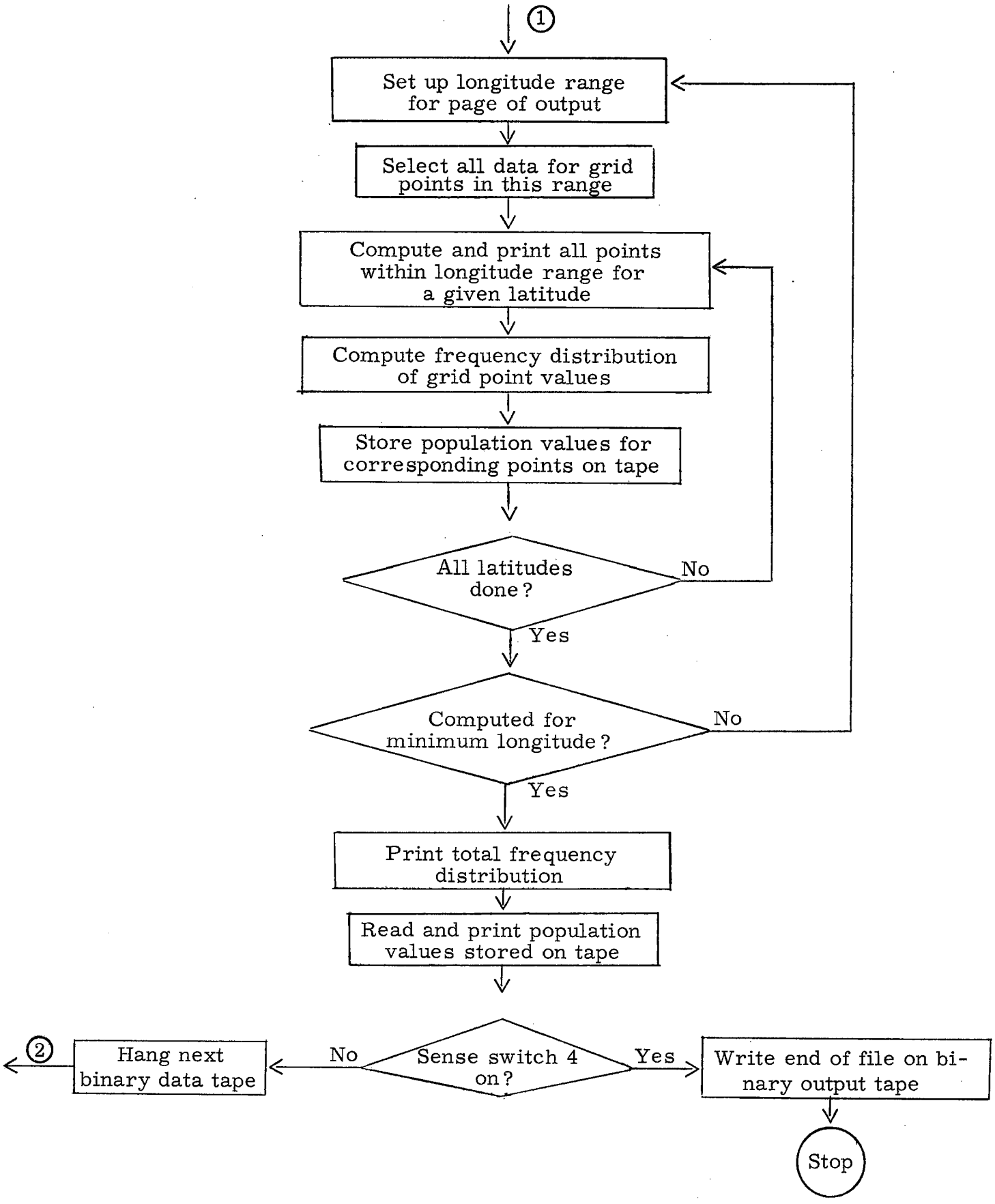
①
Set up longitude range for page of output
Select all data for grid points in this range
Compute and print all points within longitude range for a given latitude
Compute frequency distribution of grid point values
Store population values for corresponding points on tape
All latitudes done?
No
Yes
Computed for minimum longitude?
No
Yes
Print total frequency distribution
Read and print population values stored on tape
Sense switch 4 on?
No
Yes
②
Hang next binary data tape
Write end of file on binary output tape
Stop

Main Program: RADAT

Controls spacing down on the binary output tape, which saves the raw data used in the computations. Program also controls cycling for reading data, selecting maximum and minimum longitude, sets up the latitude and longitude for each grid point, and regulates the computation and printing of the frequency distribution.

Subprogram: FIRST

Spaces down the input tape to the proper orbit, reads the first documentation record, floats this information, and reads the first record of data.

Subprogram: REST

Reads subsequent record of data while unpacking the previous record.

Subprogram: SORT

Searches through a record of data for any data in the specified latitude range, floats and stores this data.

Since latitude and longitude are given only for every fifth radiation value, the intermediate latitudes and longitudes are computed.

Subprogram : P 3

Computes grid point values using the quadradic surface analysis or the weight function method, whichever is appropriate.

Subprogram: SES

Inverts the matrix formed in Subprogram P 3.

Subprogram: OUT

Prints heading for the grid of radiation values, prints longitudes along the top, latitudes along the sides and prints radiation values in form of a grid where each point is . 5 inches apart (represents . 5^{o}).

Subprogram: OUT 1

Reads population values as stored on tape and prints population map for grid points in the same format as the radiation grid.

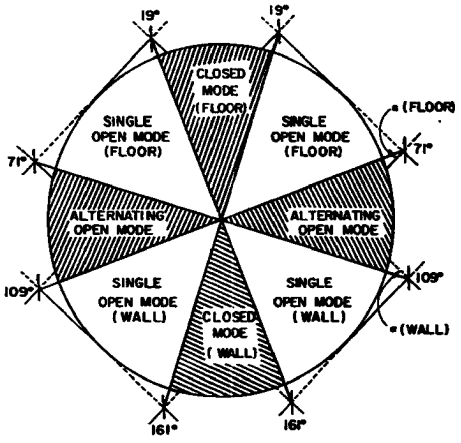

Fig. 1 Possible satellite modes and nadir angles (α) from both the floor and the wall sensors. Arrows indicate spin vector through top of satellite, solid lines at 45^{o} to the arrows indicate the floor, and dashed lines the wall scan of the radiometer (from TIROS IV Radiation Data Catalog, NASA, 1963).

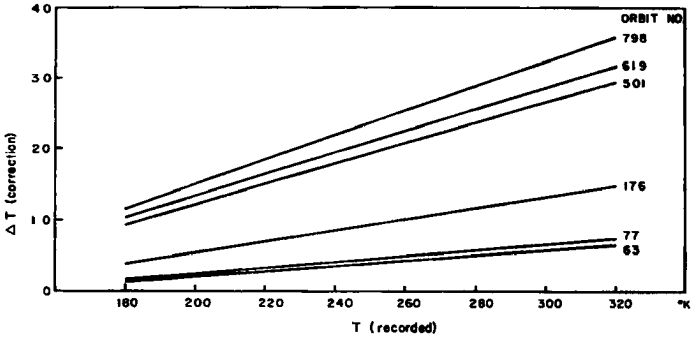

Fig. 2 Temperature correction to the recorded temperatures as a function of the recorded temperature for selected computed orbits.

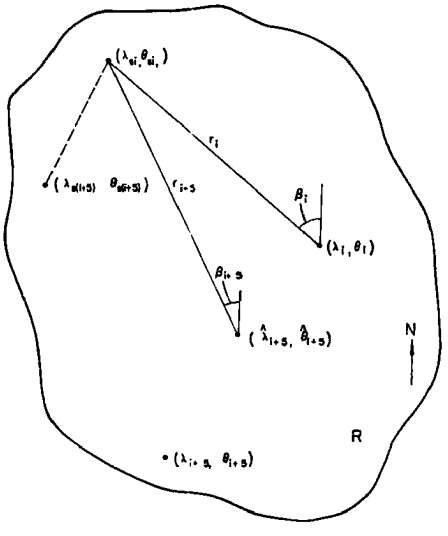

Fig. 3 Angular consideration for interpolation of non-geographically defined data points (see text). R is the region on earth including scan area.

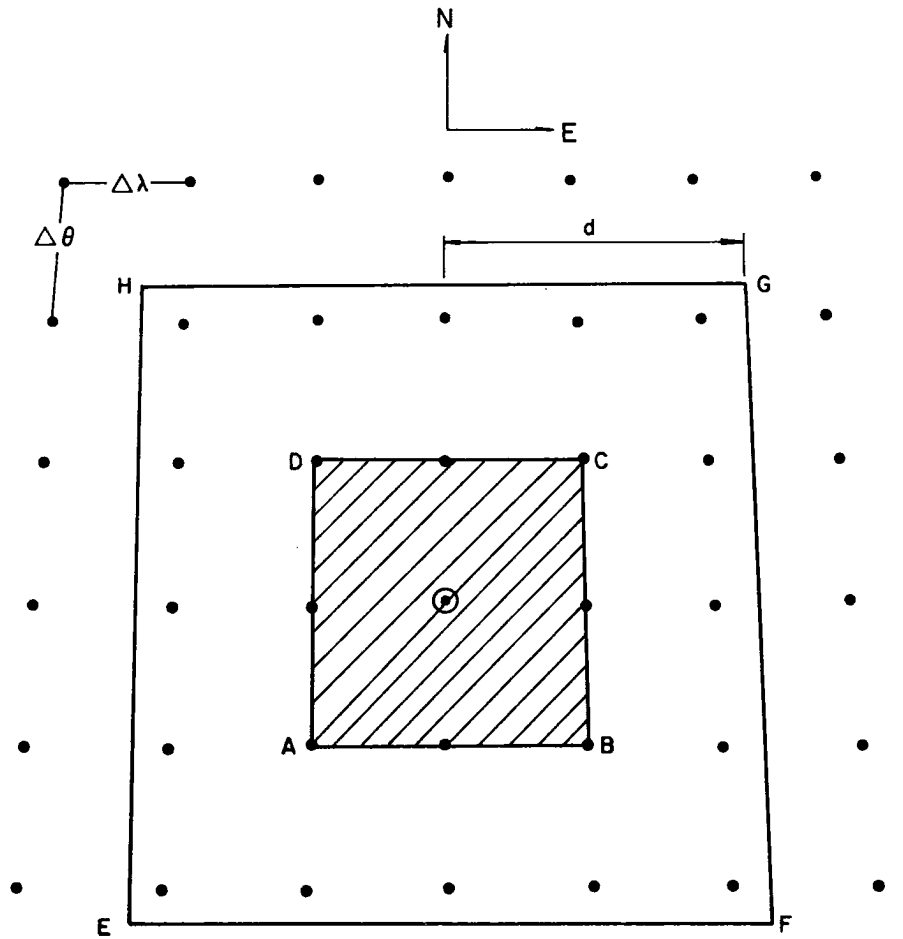

Fig. 4 Grid configuration: influence region about point 0 is bounded by the curve EFGH; center of gravity of data points must fall inside the region bounded by ABCD.

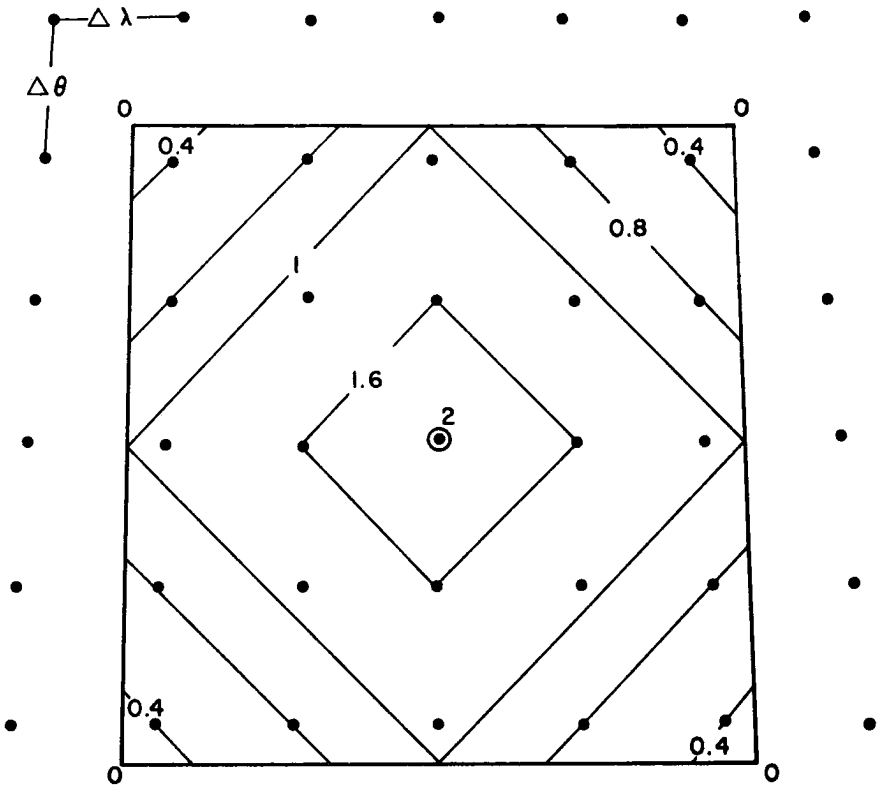

Fig. 5 Weight function (w) applied to data (about point 0) for grid point evaluation of polynominal fitting is not adequate.

Fig. 6 Map of radiation values over the selected region as seen by TIROS III during orbit number 77.

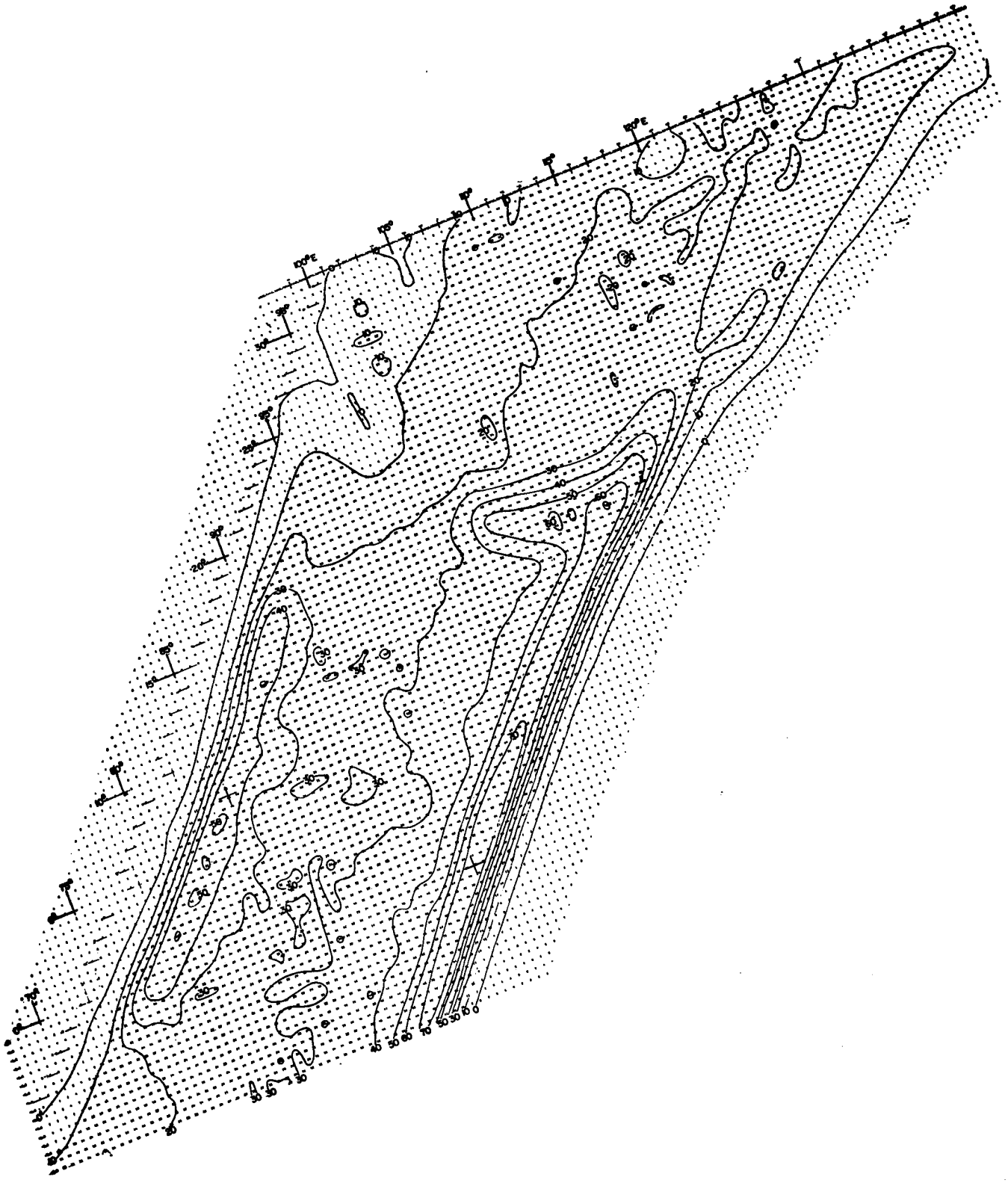

Fig. 7 Map for same region and orbit as Figure 6, showing analysis of data density in the influence region of each grid point.

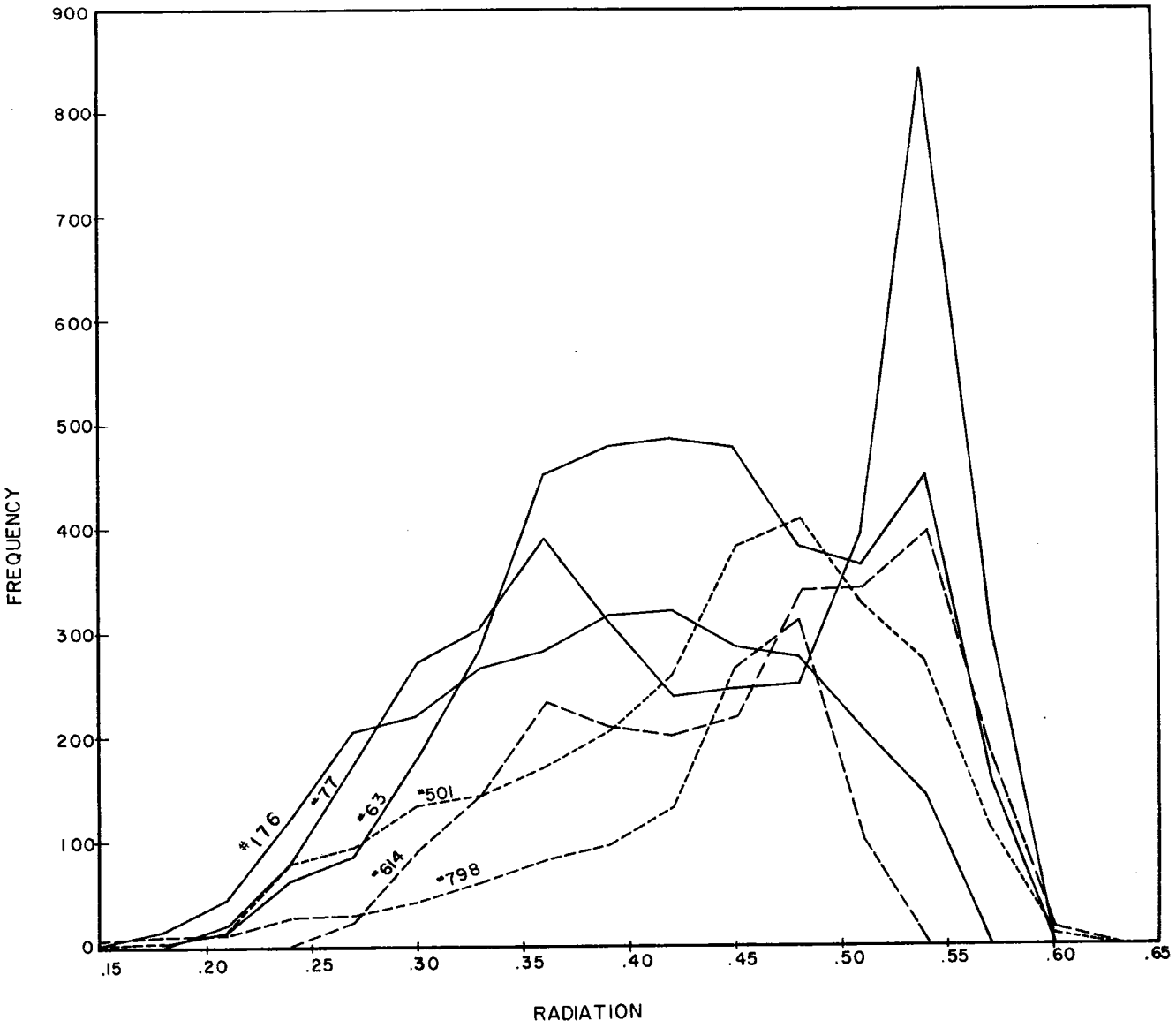

Fig. 8 Frequency distribution of radiation data for a selected number of orbits of TIROS III.

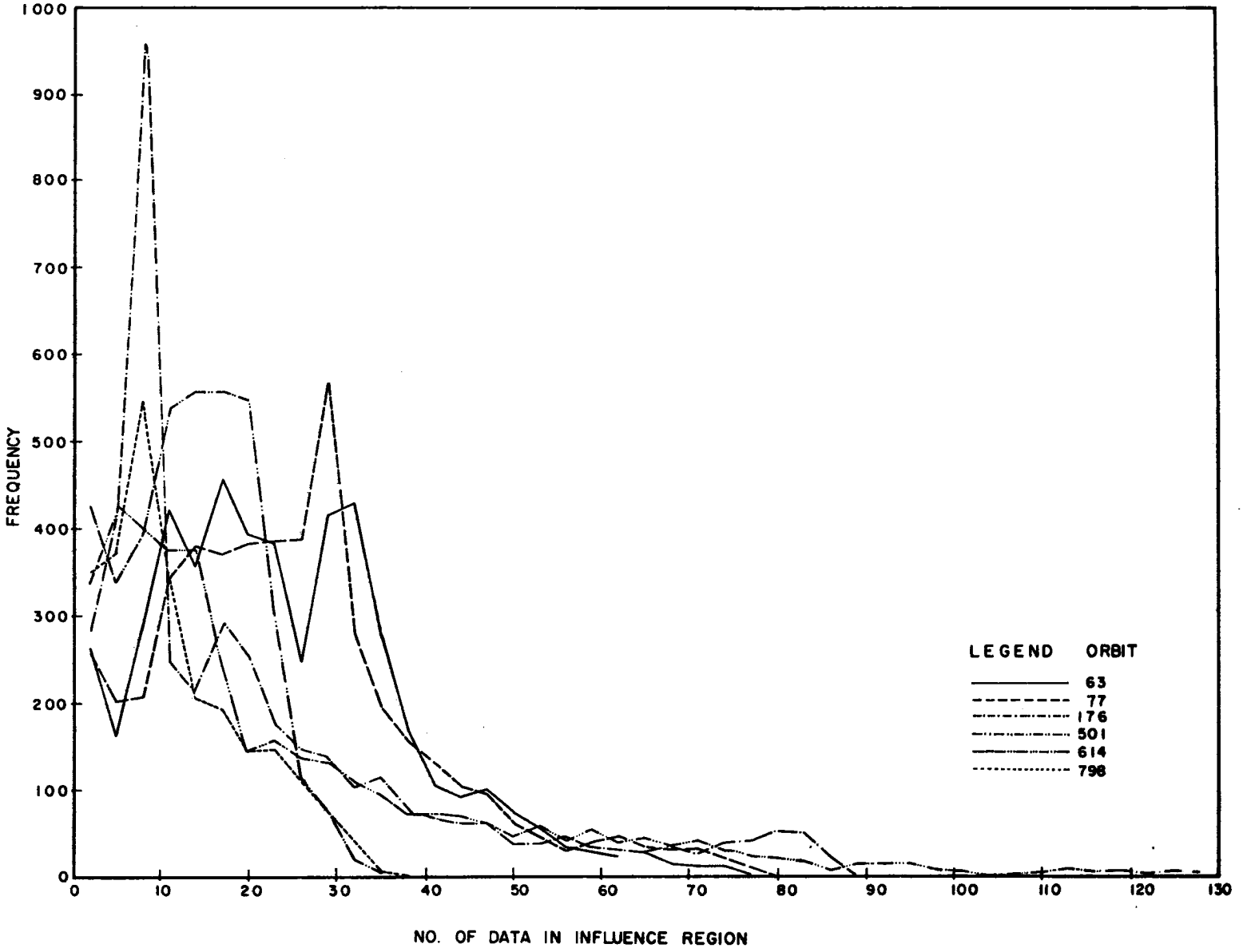

Fig. 9 Frequency distribution of the number of data points per grid point for the same orbits described in Figure 8.